RSC Advances

PAPER

View Article Online
View Journal | View Issue

Cite this: *RSC Adv.*, 2017, **7**, 40914

An efficient green-emitting $Ba_5Si_2O_6Cl_6:Eu^{2+}$ phosphor for white-light LED application

Somrita Dutta and Teng-Ming Chen *

A series of novel green-emitting $Ba_5Si_2O_6Cl_6:Eu^{2+}$ (BSOC:Eu^{2+}) phosphors were synthesized *via* the high-temperature solid-state reaction route. The phase identification, elemental distribution, reflectance spectra, luminescence, and thermal stability of the BSOC:Eu^{2+} phosphor and its applicability in white light-emitting diodes (WLEDs) were investigated in detail. The broad excitation spectrum was observed from UV to blue light which generated a broadband emission peaking at 510 nm for the present phosphor with a good quantum efficiency of 44% and thereby it is promising for solid-state lighting applications. Temperature-dependent luminescence measurements of the BSOC:Eu^{2+} phosphor from 25 °C to 250 °C were performed to obtain the thermal stability of the present phosphor. Finally, a WLED was fabricated using the green-emitting BSOC:Eu^{2+} phosphor and commercially available red and blue phosphors pumped with a 400 nm blue chip. The CIE parameters such as color coordinate, color rendering index, color correlated temperature and luminous efficacy of radiation of the fabricated LED were measured. The suitable excitation spectra, efficient and broad emission band and excellent color parameters suggest that the synthesized phosphor could be a potential material for WLED application.

Received 29th June 2017
Accepted 14th August 2017

DOI: 10.1039/c7ra07221j

rsc.li/rsc-advances

1. Introduction

Phosphor-converted white light-emitting diodes (pc-WLEDs) have gained a lot of attention around the world as sources for solid-state lighting in recent times. The use of WLEDs has been coined as the next generation lighting technology for indoor and outdoor lighting systems owing to their compact volume, energy saving characteristics, long operation lifetime and most importantly being environmentally friendly.[1–7] This has provided the drive for researchers to push their imagination and come up with more and more efficient phosphors to cater for and keep pace with the growing technology in the lighting industry. Commercially, the most followed strategy for WLEDs is to combine a blue LED chip with yellow-emitting YAG:Ce^{3+} phosphor.[8] But the process to prepare WLEDs has its fair share of drawbacks in terms of colour rendering index (CRI) and poor thermal stability, thus limiting its applications in power LEDs.[9,10] Another approach for producing WLEDs is based on combining red-, green-, and blue-emitting phosphors with a near ultraviolet (near-UV) LED chip.[11–15] Hence many new phosphors are being developed continuously that can overcome the featured drawbacks of the commercial phosphor for WLEDs.[16–20]

Eu^{2+} ion is a versatile activator that can give luminescence ranging from ultraviolet to red region depending on the host material. The electronic transition $4f^65d^1 \rightarrow 4f^7$ of Eu^{2+} is strongly sensitive to its surrounding environment, *i.e.*, symmetry, covalence, bond length, crystal-field strength.[21,22] Hence Eu^{2+}-doped suitable hosts are extensively studied because of their potential applications as phosphor materials. Silicate-based materials have been a favourable host for Eu^{2+} because of their strong absorption in the UV-to-visible spectral region, thus providing strong luminescence. Silicates are highly stable and have a rigid crystal structure with covalent Si–O bonds providing a distorted surrounding around Eu^{2+}.[23–27] If a halide ion is introduced in a silicate lattice, there is a red shift of the excitation and emission band of Eu^{2+} ions due to the strong coordination effect of the halide ion, thus strengthening the crystal-field splitting of Eu^{2+} ions. Halide-containing silicates require low synthetic temperatures and they are chemically and thermally stable which adds to their advantages for suitable host lattice for luminescence materials.[28–31] Research works related to Eu^{2+}-activated alkaline-earth halosilicates have been widely reported in literature such as $Sr_5SiO_4Cl_6:Eu^{2+}$,[32] $Ba_5SiO_4(F,Cl)_6:Eu^{2+}$,[33] and much more.[34–38]

In this work, we report a green-emitting Eu^{2+} activated $Ba_5Si_2O_6Cl_6$ (BSOC) phosphor for near-UV pumped WLED, which has broad excitation range with an intense emission at 510 nm. Luminescent properties of $Ba_5Si_2O_6Cl_6:Eu^{2+}$ (BSOC:Eu) phosphors are investigated in detail. In addition, an LED device using the BSOC:Eu phosphor with a 400 nm LED chip was fabricated to demonstrate its applicability as a colour conversion phosphor in the fabrication of WLEDs.

Department of Applied Chemistry, National Chiao Tung University, Hsinchu 30010, Taiwan. E-mail: tmchen@mail.nctu.edu.tw

2. Experimental

2.1 Materials preparation

The $Ba_5Si_2O_6Cl_6$:xEu^{2+} (x = 0.025, 0.05, 0.1, 0.15, 0.2, 0.25, 0.3) phosphors were synthesized by solid-state reaction using $BaCO_3$ (Sigma-Aldrich, >99.99%), SiO_2 (Sigma-Aldrich, >99.99%), NH_4Cl (Sigma-Aldrich, >99.99%) and Eu_2O_3 (Sigma-Aldrich, >99.99%) as starting raw ingredients. Some excess amount of NH_4Cl than required molar ratio was taken of the phosphor due to the low melting point of the material. The ingredients were mixed and ground homogeneously using a mortar pestle for hours and then the mixture was first annealed at 450 °C for 1 hour and, subsequently, heated to 900 °C for 4 hours in reducing atmosphere of H_2/N_2. Bright green colored powders were obtained after cooling the products to room temperature.

2.2 Material characterization

X-ray diffraction (XRD) patterns of the phosphors were recorded in a wide range of Bragg angle 2θ ($10° \leq 2\theta \leq 60°$) using Bruker D8 Focus XRD measuring instrument with Cu target radiation (λ = 0.154056 nm). The morphology of powders was evaluated using a scanning electron microscope (Hitachi, S-5000) attached with energy dispersive X-ray spectroscopy (EDS). The diffuse reflection (DR) spectra were obtained from Hitachi 3010 double-beam UV-vis spectrometer (Hitachi Co., Tokyo, Japan) equipped with a ø 60 mm integrating sphere, whose inner face was coated with $BaSO_4$ or Spectralon and α-Al_2O_3 was used as a standard in the measurements in the range of 250–800 nm. The luminescent properties and lifetime decay of the obtained phosphors were analyzed by FS-5 Fluorescence Spectrophotometer PL system equipped with a 150 W xenon lamp. The absorption (A) and quantum efficiency (QE) were measured by an integrating sphere whose inner face was coated with Spectralon equipped with a spectrofluorometer (Horiba Jobin Yvon Fluorolog 3-2-2). The thermal luminescence (TL) quenching was tested using a heating apparatus (THMS-600) in combination with the PL equipment.

2.3 White-light LED fabrication

A WLED device was fabricated by integrating the performance-optimized green-emitting BSOC:2%Eu^{2+} phosphor with blue-emitting $BaMgAl_{10}O_{17}$:Eu^{2+} and red-emitting $Sr_2Si_5N_8$:Eu^{2+} phosphor. For electroluminescence (EL) spectrum measurement, the mixed phosphors with a transparent silicone resin are packaged with an InGaN LED chip (λ_{max} = 400 nm).

3. Results and discussion

3.1 Phase formation and morphology

Fig. 1(a) shows the XRD patterns of BSOC:Eu^{2+} phosphors with varying Eu^{2+} concentration ranging from 0.5 to 6 mol%. All the XRD patterns match well with the reference JCPDS 40-1271. It indicates the formation of pure BSOC phase. Fig. 1(b) presents the SEM image of the $Ba_5Si_2O_6Cl_6$:Eu_x^{2+} (x = 0.1) phosphor which shows agglomerated needle-shaped particles.[39] The particle size distribution was also analyzed for the present case

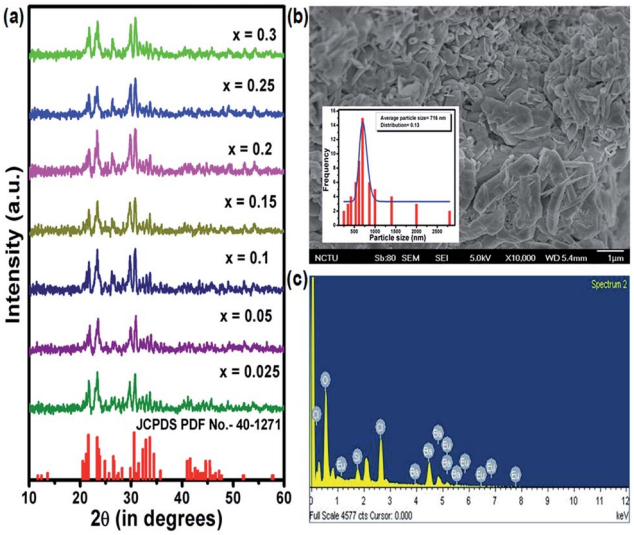

Fig. 1 (a) XRD pattern of BSOC:Eu^{2+} phosphor with the variation of Eu^{2+} concentration. (b) SEM image and (c) corresponding EDX pattern of the $Ba_5Si_2O_6Cl_6$:Eu_x^{2+} (x = 0.1) phosphor. Inset: particle size distribution of the $Ba_5Si_2O_6Cl_6$:Eu_x^{2+} (x = 0.1) phosphor.

and it was observed that the particles obeyed the lognormal behaviour[40] given by,

$$P(d) = \frac{1}{d\sigma\sqrt{2\pi}} \exp\left[\frac{-\ln^2(d/\bar{d})}{2\sigma^2}\right] \quad (1)$$

where, d and σ values indicated the average size and corresponding size distribution of the particles. From this plot, the average particle size of the phosphor was obtained as 716 nm with a narrow size distribution.

The energy dispersive X-ray spectra were also recorded for the $Ba_5Si_2O_6Cl_6$:xEu^{2+} (x = 0.1) phosphor to obtain the elemental analysis of the synthesized materials and shown in Fig. 1(c). The presence of major elements including Ba, Cl, O, Si and Eu indicates the proper formation of the material.

3.2 Diffuse reflectance and band gap

Fig. 2(a) and (b) shows the DR spectra of the undoped BSOC host and doped BSOC:Eu phosphors with the variation of Eu^{2+} ion concentration from 0.5 to 6 mol%. In both the figures the spectra show high reflection in the wavelength range 500 to 700 nm and then see a drop in the reflection intensity with a hump at around 350 nm for the doped phosphors. The results indicate the presence of two different absorptions in the UV-visible range, one is the host absorption at 300 nm which is observed from Fig. 2(a) and remains fixed for all the doping variations in Fig. 2(b) while the other is induced by the $4f^6/5d^1$ transitions of the Eu^{2+} at about 400 nm. The band gap of the phosphors was calculated using the Kubelka–Munk theory[41] using the diffuse reflectance spectra of the phosphors. The band gap (as shown in the inset of Fig. 2) for the host was found to be 4.017 eV which show a slight increase in the value to 4.04 eV for the minimum doping of 0.5 mol% to 4.09 eV for 6 mol% doping of Eu^{2+} in the host.

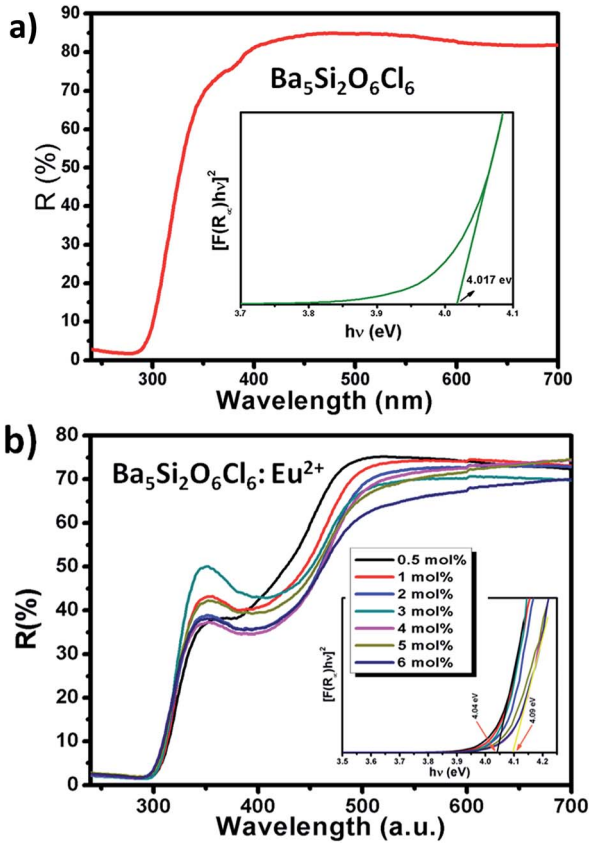

Fig. 2 DR spectra of (a) undoped BSOC, (b) BSOC:Eu^{2+} phosphor with the variation of Eu^{2+} concentration. Inset (a) and (b): estimation of band gap of undoped BSOC and BSOC:Eu^{2+} phosphor with the variation of Eu^{2+} concentration respectively.

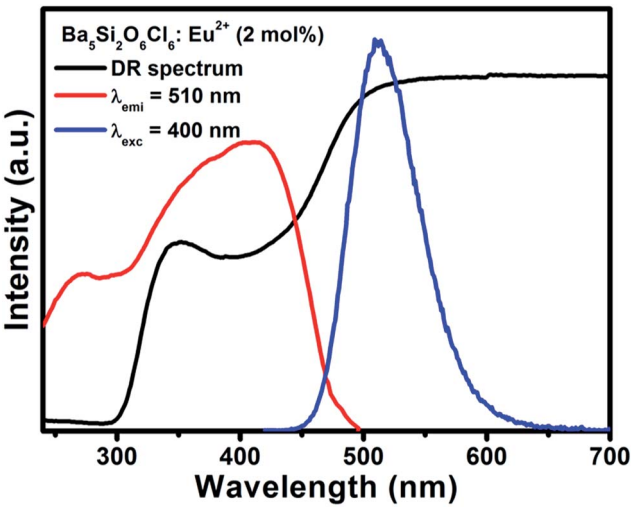

Fig. 3 DR spectra and PLE/PL spectra of BSOC:Eu^{2+} (2 mol%) phosphor.

Representative PLE/PL spectra of BSOC:Eu^{2+} (2 mol%) are shown in Fig. 3 along with the DRS spectrum to show the presence of two different absorptions. The PLE spectrum was recorded at the emission wavelength 510 nm and the PL spectrum was taken by keeping the excitation wavelength fixed at 400 nm. The PLE spectra show a small hump around 280 nm which indicates the host absorption as seen in the DRS spectrum.

3.3 Photoluminescence characterization

Fig. 4 shows the emission and excitation spectra of the $Ba_{5-x}Eu_xCl_6Si_2O_6$ phosphor varying Eu^{2+} concentration. The excitation spectra show a broad band ranging from 240 to 490 nm which is initiated by the transition from the $4f^7(^8S_{7/2})$ ground state to the $4f^65d^1$-excited level of the Eu^{2+} ions[42] with a small hump around 280 nm which can be ascribed to the host excitation. When excited at 400 nm, the emission spectra showed a broad green emission band, with a maximum at about 510 nm having an FWHM of about 66 nm. This emission can be credited to the allowed transition between the lowest relaxed $4f^65d^1$ level to the $4f^7$ ($^8S_{7/2}$) level of the Eu^{2+} ions.

Since the emission band looks symmetric in nature, hence it can be apparently said that Eu^{2+} ions occupy only one type of site in the $Ba_5Si_2O_6Cl_6$ host lattice, thus corresponding to one emission center. Generally, the local environment of Eu^{2+} is sensitive to any small modifications in the crystal disorder or deficiency of charge neutrality, so to assign an emission band to a particular crystallographic site, the famous empirical theory by Van Uitert[43] could be used. According to Van Uitert theory, the position of the d-band edge in energy for rare earth ions (E) (cm^{-1}) can be calculated using the following equation,

$$E = Q\left[1 - \left(\frac{V}{4}\right)^{\frac{1}{V}} \times 10^{nE_a r}\right] \quad (2)$$

where, Q is the position in energy for the lower d-band edge for the free Eu^{2+} ions (cm^{-1}) which is 34 000 cm^{-1}, n is the number of anions in the immediate shell around the Eu^{2+} ion, V is the valence of the Eu^{2+} ion, E_a is the electron affinity of the anionic atom (in eV), and r is the radius of the host cation replaced by the Eu^{2+} ion (in Å). Based on this, a probable solution can be obtained to know the crystallographic site substituted by Eu^{2+} ion in the BSOC lattice. By substituting specific coordination numbers into the empirical formula with the corresponding n, E_a, and r values, it can be concluded that the Ba^{2+} ions with six coordination numbers can be assigned to a single green band peaking at 510 nm, thus testifying the possible crystallographic sites in the novel BSOC:Eu^{2+} phosphor system. The result is in good agreement with the literature reported by Du *et al.*[44]

The efficient green emission with broadband nature and high excitation intensity at 350–400 nm region indicates the suitability of the BSOC phosphor as a green emitting color converter material for n-UV/blue pumped white LEDs. However, it was observed from Fig. 4 that the emission intensity of the phosphor increases with Eu^{2+} activator concentration up to 2 mol% and then decreases. The variation of the integrated PL emission intensity with the Eu^{2+} concentration is shown in Fig. 5. The reduction in PL intensity may be owing to the self concentration quenching effect of Eu^{2+} ion inside the BSOC host.

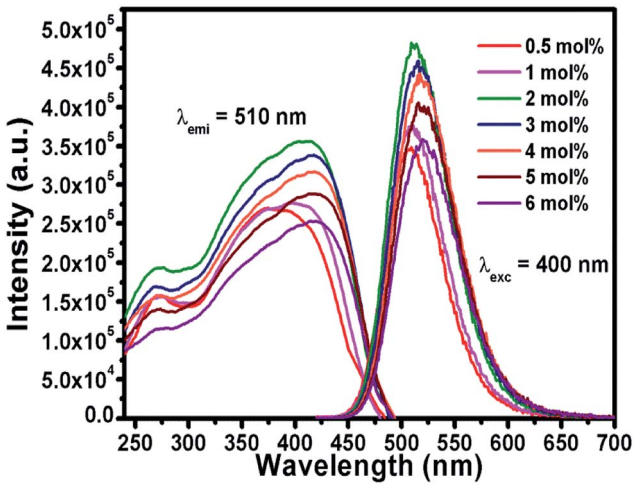

Fig. 4 PLE and PL spectra of BSOC:Eu^{2+} phosphor with the variation of Eu^{2+} concentration.

Non-radiative energy transfer between activator ions is the reason for concentration quenching in the phosphor.[45] To verify the type of interactions involved in the energy transfer, the theory of Dexter can be used which is given by[46]

$$\frac{I}{C} = \frac{k}{\beta C^{s/3}} \quad (3)$$

where I/C is emission intensity per activator ion, k and β are constants for a particular interaction, and the values of s correspond to exchange, dipole–dipole (d–d), dipole–quadrupole (d–q) and quadrupole–quadrupole (q–q) interactions are 6, 8 and 10 respectively. From the logarithmic plot using eqn (3), the slope value was obtained as 2.095 as shown in the inset of Fig. 5(a). From this, the value of s was obtained as 6.285 which is very close to the theoretical value 6. It indicates the d–d interaction is the main mechanism for the concentration quenching of Eu^{2+} in BSOC:Eu^{2+} phosphor.

The normalized PL spectrum of the BSOC:Eu^{2+} phosphors in Fig. 5(b) shows a continuous shift to the higher wavelength from 509 nm to 520 nm with increasing Eu concentration. This red shift can be primarily attributed to the difference in ion size of larger Ba^{2+} and smaller Eu^{2+} ion. Considering the crystal field strength equation:[47,48]

$$D_q = \frac{Ze^2r^4}{6R^5} \quad (4)$$

where D_q is the crystal field strength, Z is the charge or valence of the anion, e is the charge of the electron, r is the radius of the d wavefunction, and R is the distance between the central ion and its ligands.

When the concentration of Eu^{2+} ion was increased, the lattice parameters of the host decrease and consequently it increased the crystal field strength and crystal field splitting. The change of crystal field strength might increase the Stokes shift which in turn causes a red shift of the emission band. The Stokes shift was estimated from the twice value of the energy difference between the zero phonon line energy and the energy of the maximum emission. It is well known that the spectral position of the zero-phonon line can be estimated from the

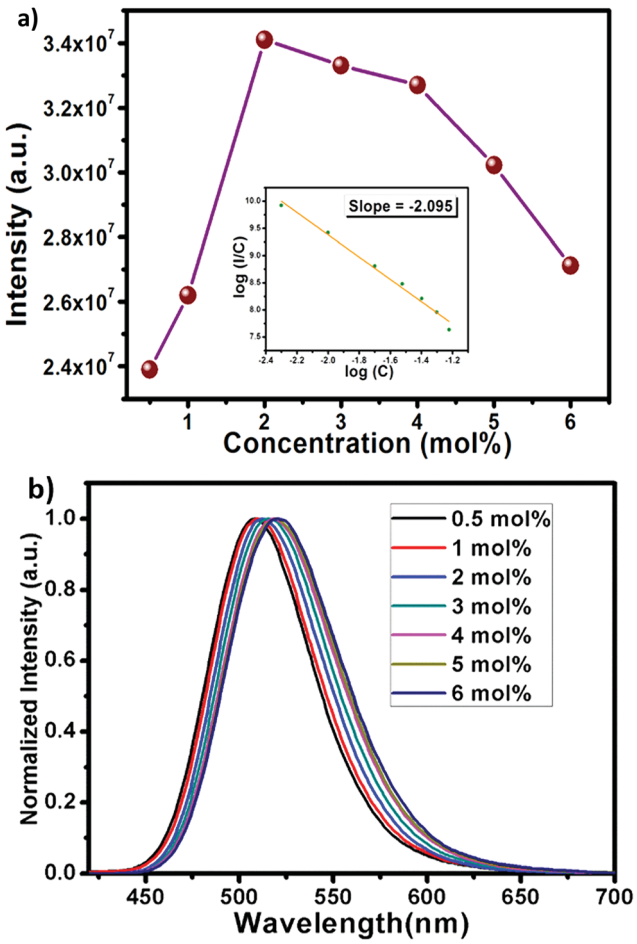

Fig. 5 (a) The variation of PL integrated emission intensity of BSOC:Eu^{2+} phosphor with the variation of Eu^{2+} concentration. Inset: logarithmic variation (I/C) with Eu^{2+} concentration in BSOC:Eu^{2+} phosphor. (b) Normalized PL spectra varying mol concentration.

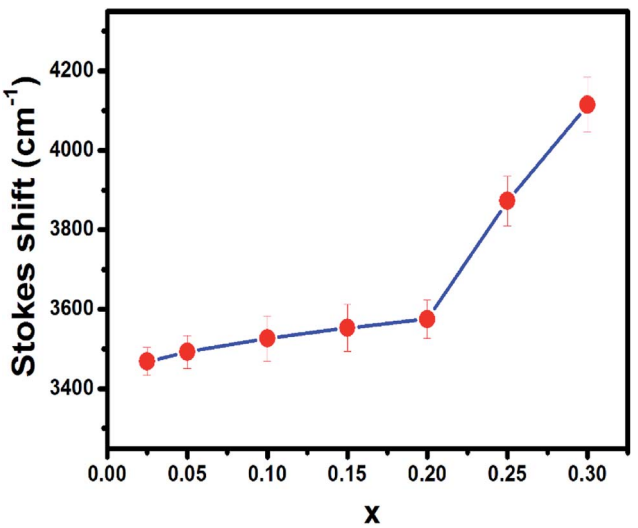

Fig. 6 The variation of Stokes shift of BSOC:Eu^{2+} phosphor with the variation of Eu^{2+} concentration.

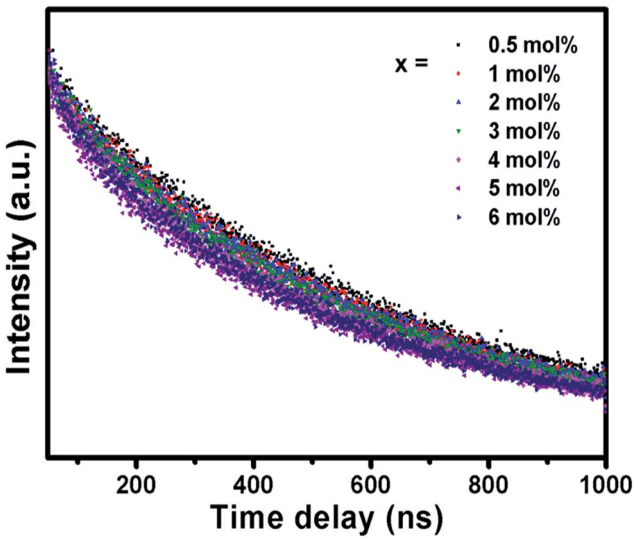

Fig. 7 The fluorescence decay curve of BSOC:Eu^{2+} phosphor with the variation of Eu^{2+} concentration.

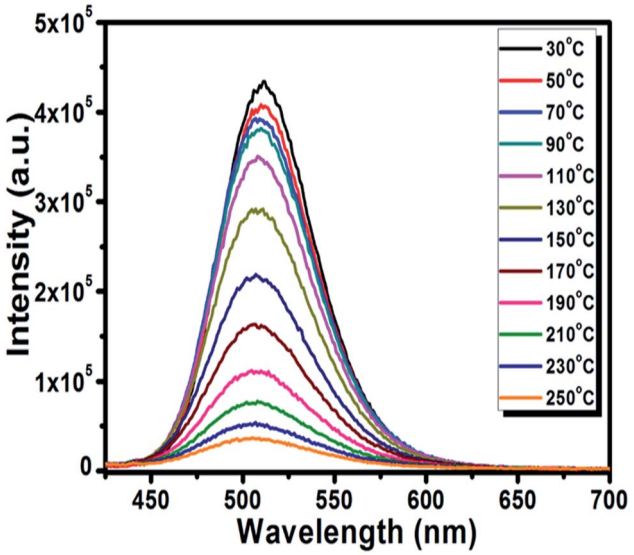

Fig. 8 The temperature-dependent PL spectra of BSOC:xEu^{2+} phosphor.

intersection of excitation and emission spectra. The modification of the Stokes shift with the variation of Eu^{2+} concentration is shown in Fig. 6. The enhancement of Stokes shift with Eu^{2+} concentration supports the red shift of the PL emission.

3.4 Decay time analysis and quantum yield

The fluorescence decay curve of the phosphors was also investigated and shown in Fig. 7. The decay curves are fitted to a single exponential decay model using the following equation,[49]

$$I = I_0 e^{\frac{-t}{\tau}} \quad (5)$$

where I and I_0 are the luminescence intensities at times t and 0, respectively, τ is the decay time. The lifetimes for the BSOC:Eu^{2+} phosphor with concentration variation are presented in Table 1. With increasing Eu^{2+} concentration, there is an increase in the rate of Eu^{2+}–Eu^{2+} energy transfer and the probability of energy transfer to quenching sites which shortens the lifetime with increasing Eu^{2+} concentration. However, the good fitting results by an exponential decay with a single component elucidate the occupancy of Eu^{2+} ions only in one site of the BSOC host, which is also consistent with the previous discussion of the eqn (2).

Table 1 The fluorescence decay life time of BSOC:Eu^{2+} phosphor with the variation of Eu^{2+} concentration

Concentration (mol%)	t (ns)
0.5	575.43
1	535.06
2	517.72
3	475.45
4	439.21
5	436.70
6	427.78

However, the internal quantum efficiency (IQE) was estimated from the well-known equation $\eta_i = N_{em}/N_{abs} \times 100\%$, where N_{abs} is the number of absorbed photons and N_{em} is the number of emitted photon. In the present research work, the Horiba Jobin Yvon Fluorolog 3-2-2 instrument was used to evaluate the internal quantum efficiency of this phosphor. The BSOC:Eu^{2+} (2 mol%) phosphor, which has maximum PL intensity, shows a respectable internal quantum yield of 44% which is comparable to the recently reported efficient phosphors.

3.5 Thermal luminescence quenching properties

The thermal stability of the phosphor is a significant parameter to evaluate its prospective use for the LED application due to its effect on the quality of light and its lifetime.[50] The temperature-dependent PL spectra of the optimized BSOC:Eu^{2+} phosphor from 30 °C to 250 °C is shown in the Fig. 8. The related PL intensity of phosphor shows a gradual decrease as the temperature increased with the broadening of the FWHM of the spectra. The similar phenomena also have been observed by other research groups.[51] The decrease is due to the increase in the population of higher vibrational levels, the density of photons and the non-radiative transfer probability with an increase in temperature.[52] The broadening of the FWHM with increase in temperature can be described by Boltzmann distribution function given by[53]

$$\mathrm{FWHM}(t) = W_0\sqrt{\coth\left(\frac{h\nu}{2kT}\right)} \quad (6)$$

where W_0 is the FWHM at 0 K, $h\nu$ is the energy of the lattice vibration that interacts with the electronic transitions. So, at higher temperatures, the interaction between the electron–phonon prevails which broadens the FWHM of the phosphor. The variation of the integrated emission intensity with the

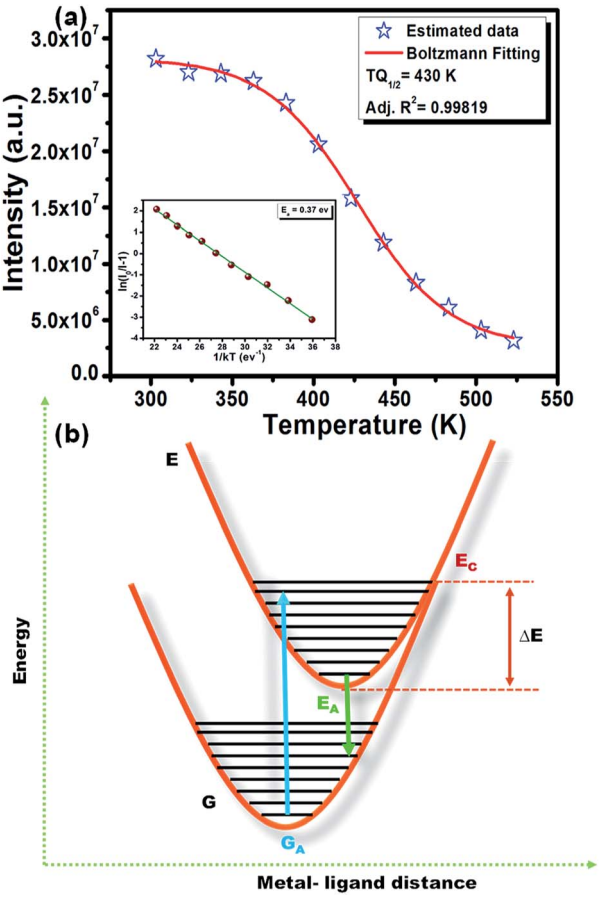

Fig. 9 (a) Variation of the integrated emission intensity with the temperature of BSOC:Eu^{2+} (2 mol%) phosphor. Inset: plot of [ln I_0/I − 1] *vs.* 1/*kT*. (b) Configuration coordinate diagram to elucidate the thermal quenching phenomena and activation energy.

temperature as shown in Fig. 9(a) follows the Boltzmann behavior. From the Boltzmann curve fitting data in Fig. 8, the value of $TQ_{1/2}$ which is the specific temperature for what the PL maxima of the phosphor was 50% of their room temperature value was obtained at 430 K (*i.e.*, 157 °C). It indicates the high stability of the present phosphor materials.

However, the decrease in luminescence intensity with the increase in temperature is generally known as thermal quenching. The temperature quenching mechanism could be explained *via* the configuration coordinate diagram as displayed in the Fig. 9(b). In this schematic diagram the *X*-axis indicates the metal–ligand distance and the *Y* axis represents the energy *E* of an absorbing center. The quantized ground state and excited state energy levels are represented *via* the parabola G and E, respectively, as indicated in the figure. The crossing point of both parabolas is displayed as the point E_C in the figure. It is well known that the phonon vibration can be reinforced with the increase in the temperature. Hence, more electrons positioned at the lowest excited state E_A can be excited to state E_C by absorbing the phonon energy. As the excited state and the ground state energy curves cross at energy E_C, the electrons at state E_C can return back to the ground state G_A by non-radiative relaxation without giving radiative emission. This surpasses the number of electrons which can return to the ground state G_A through radiation. Thus, the emission intensity of the phosphor will decrease with increasing temperature and this process is known as thermal quenching.[51,54] The energy difference between E_C and E_A is generally known as activation energy (ΔE). According to Li *et al.*[55] and Ronda[54] the probability of the thermal quenching process in strongly dependent on the energy barrier ΔE. A greater ΔE indicates the lower thermal quenching of the phosphor.[54–57] The activation energy of thermal quenching process of the phosphors can be calculated by Arrhenius equation[58]

$$I(t) = \frac{I_0}{1 + Ae^{-\frac{\Delta E}{K_B T}}} \quad (7)$$

where A is a constant, K_B is Boltzmann's constant, I_0 is the initial emission intensity measured at room temperature, $I(t)$ is the emission intensity measured at different temperatures, and ΔE is the activation energy for the thermal quenching. By experimental fitting of the data, as shown in the inset of Fig. 9(a), the activation energy ΔE was determined to be 0.370 eV. This value of the activation energy comparable to the recent reported value indicates the moderate thermal stability of the present phosphor materials to be used in high-power LEDs.

3.6 Fabrication of WLEDs

To demonstrate the potential application of $Ba_5Si_2O_6Cl_6$:Eu^{2+} for pc-WLEDs, the phosphor was used for a WLED fabrication with commercially-available red-emitting $Sr_2Si_5N_8$:Eu^{2+} (ref. 59) and a blue-emitting $BaAl_{10}MgO_{17}$:Eu^{2+} (ref. 60) with a 400 nm InGaN-based LED chip. The LED chip was operated under a forward bias voltage of 5.0 V. Fig. 10 displays the EL spectra of InGaN-based white LED device by varying driving currents in the range 100–450 mA.

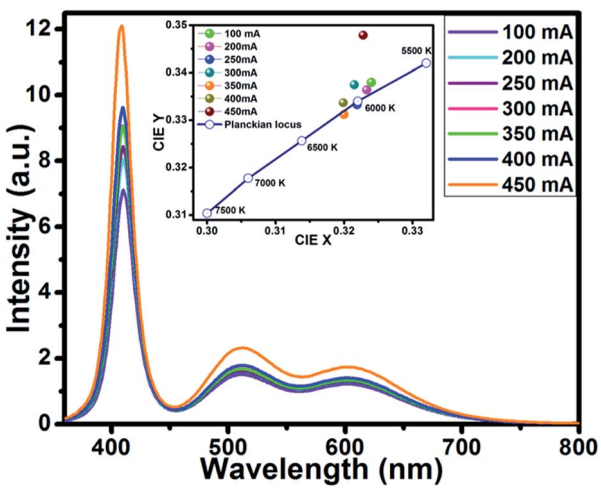

Fig. 10 EL spectra of the device using BSOC:Eu^{2+} + red phosphor + blue + 400 nm LED chip. Inset: variation in CIE chromaticity coordinates of the WLED operated under different currents (100–450 mA).

Table 2 Optical properties of the fabricated LEDs

Forward bias current I (mA)	CIE x	CIE y	CCT (K)	CRI (R_a)
100	0.324	0.338	5890	88.4504
200	0.3233	0.3333	5925	87.8862
250	0.3219	0.3364	6003	87.6355
300	0.3215	0.3375	6008	87.745
350	0.32	0.3312	6106	87.3902
400	0.3199	0.3337	6103	87.3826
450	0.3228	0.3479	5920	88.2024

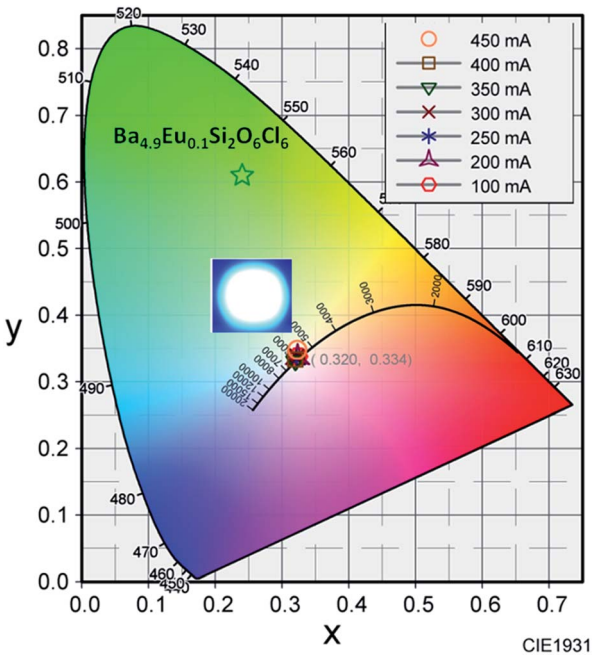

Fig. 11 Variation in CIE chromaticity coordinates as a function of forward bias current. Inset: LED device photograph.

With the increase in forward biased current from 100 mA to 450 mA, the EL intensity was found increasing without getting saturated. The optical properties of the fabricated WLED device such as the CIE coordinates, CRI and CCT of the phosphor are presented in Table 2.

The inset of Fig. 10 shows the variation of CIE chromaticity coordinates with varying current which shows very slight shift of the coordinates as also depicted in the Table 2. Fig. 11 displays the CIE colour coordinate diagram which shows the stability of the colour emission in the white region with increasing forward bias current.

The colour coordinate of the 2 mol% Eu^{2+} activated BSOC phosphor is also shown in the Fig. 11. The digital image of fabricated WLEDS indicates warm white light emission. The results established the excellent color stability with high CRI and good CCT of the BSOC:Eu^{2+} phosphor with different driving currents. Thus, in comparison to the low CRI and high CCT of the commercially used $Y_3Al_5O_{12}$:Ce^{3+} phosphor for WLEDs, the white light produced in this work retains high CRI and lower colour temperature. The performance of the WLED device can be further improved by controlling the operating parameters precisely during device fabrication.

4. Conclusion

A series of novel green-emitting Eu^{2+} doped $Ba_5Si_2O_6Cl_6$ phosphors were synthesized *via* solid-state reaction route. The diffuse reflectance spectroscopy was used to estimate the band gap of the phosphors. The detailed luminescence studies were carried out to study the applicability of the phosphor in W-LEDs. The broad excitation spectra from NUV-blue region and corresponding symmetrical green emission band with high efficiency were obtained. Eu^{2+} ions occupy only one type of site in the $Ba_5Si_2O_6Cl_6$ host lattice, thus corresponding to one emission center. The concentration quenching for the Eu^{2+} ions in BSOC host was observed at 2 mol% due to dipole–dipole interaction between the Eu^{2+} ions. Excellent thermal stability and suitable lifetime and relatively high quantum efficiency was obtained for the optimized phosphor. The LED fabricated using this phosphor along with commercial red and blue phosphor excited by a 400 nm InGaN LED chip showed high CRI value and lower colour temperature along with excellent colour stability with forward bias current variation. All the studies indicate the BSOC:Eu^{2+} phosphor to be a prospective candidate for WLEDs for the generation of warm white light.

Conflicts of interest

There are no conflicts of interest to declare.

Acknowledgements

The present work was supported by the Ministry of Science and Technology of Taiwan under the contract No. MOST 105-2811-M-009-085 and MOST 104-2113-M-009-018-MY3.

References

1 S. Pimputkar, J. S. Speck, S. P. Den Baars and S. Nakamura, *Nat. Photonics*, 2009, **3**, 179–181.
2 T. Justel, H. Nikol and C. Ronda, *Angew. Chem., Int. Ed.*, 1998, **37**, 3084–3103.
3 R. J. Xie, N. Hirosaki, T. Suehiro, F. F. Xu and M. Mitomo, *Chem. Mater.*, 2006, **18**, 5578–5583.
4 L. Chen, R. H. Liu, W. D. Zhuang, Y. H. Liu, Y. S. Hu, X. F. Zhou and X. L. Ma, *J. Alloys Compd.*, 2015, **627**, 218–221.
5 S. Som, P. Mitra, V. Kumar, V. Kumar, J. J. Terblans, H. C. Swart and S. K. Sharma, *Dalton Trans.*, 2014, **43**, 9860–9871.
6 A. A. Setlur, W. J. Heward, M. E. Hannah and U. Happek, *Chem. Mater.*, 2008, **20**, 6277–6283.
7 C. Feldmann, T. Justel, C. R. Ronda and P. J. Schmidt, *Adv. Funct. Mater.*, 2003, **13**, 511–516.
8 Y. C. Jia, Y. J. Huang, Y. H. Zheng, N. Guo, H. Qiao, Q. Zhao, W. Z. Lv and H. P. You, *J. Mater. Chem.*, 2012, **22**, 15146–15152.

9 J. S. Kim, P. E. Jeon, J. C. Choi and H. L. Park, *Appl. Phys. Lett.*, 2004, **84**, 2931–2933.
10 J. K. Park, M. A. Lim, C. H. Kim and H. D. Park, *Appl. Phys. Lett.*, 2003, **82**, 683–685.
11 J. K. Sheu, S. J. Chang, C. H. Kuo, Y. K. Su, L. W. Wu, Y. C. Lin, W. C. Lai, J. M. Tsai, G. C. Chi and R. K. Wu, *IEEE Photonics Technol. Lett.*, 2003, **15**, 18–20.
12 Y. Chen, F. Pan, M. Wang, X. Zhang, J. Wang, M. Wu and C. Wang, *J. Mater. Chem. C*, 2016, **4**, 2367–2373.
13 Y. Liu, X. Zhang, Z. Hao, X. Wang and J. Zhang, *Chem. Commun.*, 2011, **47**, 10677–10679.
14 C. H. Huang, P. J. Wu, J. F. Lee and T. M. Chen, *J. Mater. Chem.*, 2011, **21**, 10489–10495.
15 F. Xie, J. Li, Z. Dong, D. Wen, J. Shi, J. Yan and M. Wu, *RSC Adv.*, 2015, **5**, 59830–59836.
16 D. Geng, M. Shang, D. Yang, Y. Zhang, Z. Cheng and J. Lin, *Dalton Trans.*, 2012, **41**, 14042–14045.
17 Y. C. Chiu, W. R. Liu, C. K. Chang, C. C. Liao, Y. T. Yeh, S. M. Jang and T. M. Chen, *J. Mater. Chem.*, 2010, **20**, 1755–1758.
18 Z. Xia and A. Meijerink, *Chem. Soc. Rev.*, 2017, **46**, 275–299.
19 Z. Xia and Q. Liu, *Prog. Mater. Sci.*, 2016, **84**, 59–117.
20 Z. Xia, Z. Xu, M. Chen and Q. Liu, *Dalton Trans.*, 2016, **45**, 11214–11232.
21 H. J. Kim, S. Unithrattil, Y. H. Kim, W. J. Chung and W. B. Im, *RSC Adv.*, 2017, **7**, 2025–2032.
22 D. Y. Wang, Y. C. Wu and T. M. Chen, *J. Mater. Chem.*, 2011, **21**, 18261–18265.
23 Y. Shimomura, T. Honma, M. Shigeiwa, T. Akai, K. Okamoto and N. Kijima, *J. Electrochem. Soc.*, 2007, **154**, J35–J38.
24 T. Abe, K. Toda, K. Uhematsu, M. Sato, T. Ishigaki, K. B. Sung, D. S. Jo, T. Masaki and D. H. Yoon, *Key Eng. Mater.*, 2014, **582**, 214–217.
25 S. Ray, Y. C. Fang and T. M. Chen, *RSC Adv.*, 2013, **3**, 16387–16391.
26 I. Baginskiy, R. S. Liu, C. L. Wang, R. T. Lin and Y. J. Yao, *J. Electrochem. Soc.*, 2011, **158**, 118–121.
27 J. Chen, C. Guo, Z. Yang, T. Li and J. Zhao, *J. Am. Ceram. Soc.*, 2015, 1–8.
28 W. J. Yang, L. Luo, T. M. Chen and N. S. Wang, *Chem. Mater.*, 2005, **17**, 3883–3888.
29 D. S. Jo, Y. Y. Luo, K. Senthil, K. Toda, B. S. Kim, T. Masaki and D. H. Yoon, *Opt. Mater.*, 2012, **34**, 696–699.
30 W. B. Im, Y. I. Kim and D. Y. Jeon, *Chem. Mater.*, 2006, **18**, 1190–1195.
31 J. Wang, L. Qin, Y. Huang, D. Wei and H. J. Seo, *Appl. Phys. A*, 2014, **115**, 1215–1221.
32 C. Fouassier and R. Romano, *US Pat.* 5, 124, 564, 1992.
33 A. Garcia, B. Latourrette and C. Fouassier, *J. Electrochem. Soc.*, 1979, **126**, 1734–1736.
34 W. Ding, J. Wang, Z. Liu, M. Zhang, Q. Su and J. Tang, *J. Electrochem. Soc.*, 2008, **155**, J122–J127.
35 J. Wang, G. Li, S. Tian, F. Liao and X. Jing, *Mater. Res. Bull.*, 2001, **36**, 2051–2057.
36 Z. Xia, Q. Li and J. Sun, *Mater. Lett.*, 2007, **61**, 1885–1888.
37 H. Y. Koo, S. K. Hong, J. M. Han and Y. C. Kang, *J. Alloys Compd.*, 2008, **457**, 429–434.
38 C. Guo, M. Li, Y. Xu, T. Li and J. Bai, *Appl. Surf. Sci.*, 2011, **257**, 8836–8839.
39 Y. K. Mishra, S. Kaps, A. Schuchardt, I. Paulowicz, X. Jin, D. Gedamu, S. Freitag, M. Claus, S. Wille, A. Kovalev, S. N. Gorb and R. Adelung, *Part. Part. Syst. Charact.*, 2013, **30**, 775–783.
40 S. Som, S. K. Sharma and S. P. Lochab, *Phys. Status Solidi A*, 2013, **210**, 1624–1635.
41 S. Som and S. K. Sharma, *J. Phys. D: Appl. Phys.*, 2012, **45**, 415102.
42 S. J. Gwak, P. Arunkumar and W. B. Im, *J. Phys. Chem. C*, 2014, **118**, 2686–2692.
43 L. G. Van Uitert, *J. Lumin.*, 1984, **29**, 1–9.
44 H. Du, J. Sun, Z. Xia and J. Sun, *Appl. Phys. B*, 2009, **96**, 459–463.
45 S. Dutta, S. Som and S. K. Sharma, *Dalton Trans.*, 2013, **42**, 9654–9661.
46 G. Blasse, *J. Solid State Chem.*, 1986, **62**, 207–211.
47 P. Dorenbos, *J. Lumin.*, 2003, **104**, 239–260.
48 H. Jang, W. Im, D. Lee, D. Jeon and S. Kim, *J. Lumin.*, 2007, **126**, 371–377.
49 S. Som, S. Das, S. Dutta, H. G. Visser, M. K. Pandey, P. Kumar, R. K. Dubey and S. K. Sharma, *RSC Adv.*, 2015, **5**, 70887–70898.
50 Y. Li, J. Wang, Y. Huang and H. J. Seo, *J. Am. Ceram. Soc.*, 2010, **93**, 722–726.
51 M. Zhang, Y. Liang, S. Xu, Y. Zhu, X. Wu and S. Liu, *CrystEngComm*, 2016, **18**, 68–76.
52 R.-J. Xie, N. Hirosaki, N. Kimura, K. Sakuma and M. Mitomo, *Appl. Phys. Lett.*, 2007, **90**, 191101.
53 J. Kim, Y. Park, S. Kim, J. Choi and H. Park, *Solid State Commun.*, 2005, **133**, 445–448.
54 C. Ronda, *Luminescence: From Theory to Applications*, WILEY-VCH Verlag GmbH & Co. KGaA, Weinheim, 2007.
55 W. Li, R.-J. Xie, T. Zhou, L. Liu and Y. Zhu, *Dalton Trans.*, 2014, **43**, 6132–6138.
56 K. Shioi, N. Hirosaki, R.-J. Xie, T. Takeda and Y.-Q. Li, *J. Mater. Sci.*, 2010, **45**, 3198–3203.
57 S. Shionoya and W. M. Yen, *Phosphor Handbook, laser & optical science and technology series*, CRC, New York, 1998.
58 Y. Chen, F. Pan, M. Wang, X. Zhang, J. Wang, M. Wu and C. Wang, *J. Mater. Chem. C*, 2016, **4**, 2367–2373.
59 R. J. Xie, N. Hirosaki, T. Suehiro, F. F. Xu and M. Mitomo, *Chem. Mater.*, 2006, **18**, 5578–5583.
60 C. H. Huang, Y. C. Chiu, Y. T. Yeh, T. S. Chan and T. M. Chen, *ACS Appl. Mater. Interfaces*, 2012, **4**, 6661–6668.